Effect of substrate temperature and electrolyte composition on the fabrication of through-hole porous AAO membrane with SF-MDC

Adane Adugna Ayalew[a*], Xiaole Han[a], and Masatoshi Sakairi[b]

[a] Graduate School of Engineering, Hokkaido University, Kita-13, Nishi-8, Kita-Ku, Sapporo 060-8628, Japan

[b] Faculty of Engineering, Hokkaido University, Kita-13, Nishi-8, Kita-Ku, Sapporo 060-8628, Japan

* Corresponding author email: adaneadugna.ayalew.j9@elms.hokudai.ac.jp

Adane Adugna AYALEW: adaneadugna.ayalew.j9@elms.hokudai.ac.jp

Xiaole HAN: hansyole@eis.hokudai.ac.jp

Masatoshi SAKAIRI: msakairi@eng.hokudai.ac.jp

Abstract

Fabrication of novel nanostructure materials on various metal substrates receives large attensions for numerous industrial applications. In this research, the influence of substrate temperature and electrolyte composition on pore parameters and oxide film thickness of anodic porous alumina (AAO) were studied. A 3D-printed solution-flow type microdroplet cell (SF-MDC) was used for the fabrication of AAO membranes in aluminum substrate. Alumina lines were formed at a constant applied voltage. The temperature of the substrate was controlled with a thermoelectric Peltier device system in the range of 10 ˚C to 60 ˚C. The surface and cross-section morphology of the anodic oxide lines were observed using a scanning electron microscope (SEM). The result showed that the pore diameter and interpore distance of the anodized lines increased as the substrate temperature increased. A highly ordered with hexagonal pore arrangement and lowest film thickness were obtained at the highest substrate temperature of 60 ˚C. The porous AAO membrane film thickness formed in the oxalic acid electrolyte increased from 32.2 μm to 52.5 μm as the anodizing substrate temperature reached 30 ˚C and then declined to 12.8 μm with increasing temperature to 60 ˚C. A through-hole porous AAO membranes were successfully fabricated at constant applied voltage and room temperature in oxalic and phosphoric acid without chemical etching.

Keywords: Alumina; Anodizing; Temperature; Through-hole; 3D-printed

1. Introduction

Currently, the fabrication of numerous nanostructured materials and their commercial applications have drawn considerations [1]. Several electrochemical patterning techniques, such as lithography, masking, and coating, have emerged to fabricate porous anodic aluminum oxide (AAO) layers on aluminum (Al) substrates [2]. However, it is difficult to produce self-ordered nanostructures using conventional optical lithography techniques on length scales smaller than hundreds of nanometers. Advanced non-optic lithographic methods, such as X-ray, ion-beam, electron-beam, imprinting, and interference lithography, are more adequate to be used effectively for the fabrication of nanostructured materials at the nanometers scale [3]. However, these techniques are not widely used due to the complicated facilities that are needed during the fabrication process. The applicability of these techniques is restricted due to additional disadvantages like high cost and a poor aspect ratio of the generated nanostructure.

Recent localized electrochemical fabrication techniques such as atomic force microscopes (AFM), scanning tunning microscopes (STM), and scanning electrochemical microscope (SECM) have been widely used to manufacture nanostructures on selective substrate areas [4] [5]. These methods are better than traditional lithographic and masking methods because they use a precisely defined area, need a minimal amount of electrolyte, and do not require any prior preparation of the substrate. The study on the fabrication technique of porous AAO membrane has been performed recently by many researchers using various techniques. Among those electrochemical fabrication techniques, electrochemical droplet cell techniques are getting specific consideration for localizing oxide lines on selective substrate areas [6] [7] [8]. A 3D-printed solution flow-type microdroplet cell (SF-MDC) is a recent new electrochemical fabrication technique that has been developed for electrochemical deposition and local anodized patterns on various metal substrates [1] [9] [10]

[11]. This technique allows for the fast fabrication of various micro-and nano-structure materials on the selective substrate area.

Fabrication of high-ordered porous AAO films on various selective substrate surfaces has received a significant application in the fabrication of capacitors, electronic circuits, sensors, resistors, and separations [12] [13]. Pore characteristics such as pore diameter, interpore distance, pore density, pore length, and barrier film thickness significantly influence the performance of the fabricated porous AAO membrane. These pore parameters strongly depend on the composition and concentration of the electrolyte, applied voltage, current density, anodizing temperature, and anodizing time. In most studies, the influence of anodizing temperature is usually investigated by varying the electrolyte temperature. However, the effect of local substrate temperature over heating when the current passes through the substrate has been inadequately studied.

Anodizing temperature is an important factor for the formation of self-ordered porous AAO and oxide layer growth. It was reported that a highly ordered porous AAO membrane was achieved at an appropriate fabrication condition [14]. Currently, many researchers conduct experiments at high electrolyte temperatures to obtain the optimum conditions for fast growth of self-ordered anodic alumina membranes. Increasing the electrolyte temperature causes a high rate of chemical dissolution and local burning of the oxide film [15]. During Al anodizing, thermal effects such as joule heating due to the flow of current in the substrate and the thin layer at the bottom of the pore can occur. Chemical reactions such as an endothermic reaction of Al_2O_3 dissolution and an exothermic reaction of Al oxidation also occurred. Moreover, the electrolyte temperature also mainly influences the oxidation reaction of Al by accelerating the flow of O^{2-} and Al^{3+} ions from the barrier film within the electric-field and enhancing the chemical dissolution of each pore wall to form regular and high-order porous morphology. It was also reported that the temperature of

anodic alumina layer at the oxide/Al interface is higher than that at the electrolyte/oxide interface because of the low thermal conductivity and heat generation of the alumina [16]. Subsequently, the temperature of the anodized alumina surface film is lower than the inside of the alumina. Even though most studies are dedicated to the examination of the effect of electrolyte temperature, some authors studied the temperature of the substrate on the oxide morphology. Chernyakova et al. [17] studied the effect of Al anode temperature on the growth of anodic alumina and the morphology of porous anodic film. The temperature of the Al substrate was controlled with the thermoelectric Peltier devices in the range of 5 ˚C to 60 ˚C. In their study, alumina was formed in in an aqueous solution of 0.4 M oxalic acid at a constant electrolyte temperature and applied voltage. The pore diameter and interpore distance significantly have not altered as the substrate temperature was increased while the anodized pore structure became highly ordered. Aerts et al. [18] also investigated the influence of control electrode temperature in the range of 5-65 ˚C on porous alumina layer growth on Al. The electrode temperature was controlled by a thermostatic holder through the Peltier effect. The authors confirmed that anodizing at high electrode temperatures results in a disordered porous structure at the alumina surface. At constant electrolyte temperature, the anodized oxide film thickness decreases with rising electrode temperature. The thermal conductivity of the specimen affected the dissipation of heat, which1 indirectly influenced the rate of oxide layer dissolution and pore structure. During the anodizing process, substrate temperature can influence the electrochemical oxidation of Al and result in an alteration of the surface morphology of oxide layers. The flow of ions in the electrolyte droplets and across the barrier layer, as well as the heat dissipation within the AAO membrane during the anodizing process, are all influenced by the temperature of the substrate.

In the conventional anodizing approach, through-hole porous AAO is produced through post-treatment procedures by applying wet-chemical etching to remove the barrier-type oxide film. This pore opening process approach has drawbacks and influences the morphology and pore size of the AAO membrane [19]. During post-treatment, when the exposed oxide barrier layer is more dissolved in strong acids such as phosphoric acid or etched with ions, it results in undesired pore widening, making it unviable to use on large-scale applications. Most parts of the porous AAO membrane collapse and are complete damaged after a long duration of chemical etching [20].

The through-hole-pore AAO membrane prepared using the SF-MDC technique is mainly done by controlling the scanning speed and number of cycling or back-and forth movements. Compared to the conventional anodized method, SF-MDC is area-selective and environmentally friendly process because it does not apply chemical etching during pore opening. Fabrication of AAO membrane with a high pore density and a small pore size achieved using SF-MDC is essential for maximizing the permeation rate and molecular flux through the membrane in the application of fluid separation. Sakairi et al. [21] developed for the first time a dual capillary SF-MDC for local anodizing of the alumina membrane, and later studied by Bilal and Sakairi [22] who proposed 3D-printed SF-MDC for localized anodizing of two different areas on the Al surface to form a porous-type anodic oxide layer in oxalic acid. Even though porous AAO was successfully fabricated on Al substrate, the influence of anodize substrate temperature and electrolyte composition on pore parameters and the formation of a through-hole anodic membrane has not been reported.

In this study, a new design of 3D-printed SF-MDC was used for fabrication of a through-hole porous AAO membrane within controlled pore sizes. The influence of substrate temperatures

and electrolyte compositions on the formation of open-pore-type porous AAO membrane pore structure parameters and film thickness were primarily investigated.

2. Experimental

2.1. Material and solution

Aluminum specimen (99.99 % mass and 300 μm thickness) was used as substrate. The specimen of aluminum was received and cut into small specimens with sizes of 20 x 30 mm. A 0.3 M oxalic acid ($C_2H_2O_4 \cdot 2H_2O$), phosphoric acid (H_3PO_4), and sulfuric acid (H_2SO_4) solution were prepared to be used as anodizing electrolytes. A 50 μm and 500 μm in diameter Pt wires were used as the counter electrodes.

2.2. Pretreatment

The Al specimens were pretreated in a 0.01 M NaOH solution for 300 s at room temperature. Then, the specimen was carefully rinsed in purified water. After being alkaline etched, the specimen was then ultrasonically cleaned using both ethanol and highly purified water, each for 300 s. After this stage, the specimen was then dried in open air and kept in a desiccator through a silica gel layer for anodizing.

2.3. Anodization

Single-capillary SF-MDC was designed using CAD software and fabricated using a 3D printer. The detailed information about the design and making process of SF-MDC was explained in previous research work [1]. The schematic setup of the anodizing process by SF-MDC is shown in Fig. 1. A clean and dried Al specimen was placed on a computer controlled XYZ stage. The electrolyte solution inlet of the SF-MDC was connected to the peristatic pump rubber tube to supply fresh electrolyte solution into the inner capillary. A droplet of electrolyte was formed at the tip of the inner capillary by controlling the electrolyte feed flow rate to 2.0 mL/s. The used solution

was continuously removed through the outer capillary at a constant vacuum pressure of 85 kPa. The electrolyte solution droplet formed at the inner capillary tip was used to form porous anodic alumina lines by moving the stage at a constant scanning speed of 3.3 μms^{-1} and a 3 mm scanning distance during anodizing. The distance between the Al specimen and the inner tip capillary was controlled to about 180 μm. Subsequently, the droplet was allowed to contact the Al substrate surface, and anodizing was conducted with an equal concentration of 0.3 M $C_2H_2O_4$, H_3PO_4, and H_2SO_4 at a constant voltage of 50 V, 170 V, and 25 V, respectively. All experiments were carried out at a constant electrolyte temperature, and the temperature of the Al specimen varied in the range of 10 ˚C to 60 ˚C by controlled with a thermoelectric Peltier device. Based on the Peltier effect, it can transfer heat into or remove heat from the Al substrate, depending on the polarization. Thus, the temperature will either be heated or cooled on the substrate surface, respectively. A Pt wire (50 μm) was inserted in the inner capillary and connected with another Pt wire (500 μm) to use as a counter electrode.

2.4. Observation

The surface images of the anodized lines were observed with an optical microscope (XV-330, WRAYMER INC., Osaka, Japan). The surface morphology and cross-sectional view of the anodized lines were investigated using a scanning electron microscope (SEM, JEOL, JSL6510-LA, Tokyo, Japan) equipped with an energy-dispersive X-ray spectroscopy (EDS) analyzer. Thin Au lyer was sputered on the anodized surface before SEM observation (Fin Coater, JFC 1600, JOEL, Tokoyo, Japan). An image processing program called “ImageJ Software [23] was used to determine the pore diameter (Dp) and interpore distance (Din), derived from SEM micrographs. The AAO layer thicknesses were measured from a cross-sectional SEM image. The pore diameter, interpore distance, and porosity of the porous AAO membrane at various substrate temperature

were evaluated. The porosity (P) of the fabricated porous AAO membrane was determined using Eq. (1) [24].

$$P(\%) = \left(\frac{\pi}{2\sqrt{3}}\right)\left(\frac{Dp}{Din}\right)^2 \times 100\ \% - - - - - - - - - - - - - - (1)$$

Where Dp is the pore diameter and Din is the inter-pore distance.

3. Results and discussion

3.1. Effect of substrate temperature on pore structure and film thickness

Using the SF-MDC technique, an attempt was made to fabricate different anodized lines with various pore diameters and alumina film thicknesses at different substrate temperatures. The effect of anodizing substrate temperature on the structure of porous AAO membrane morphology, mainly on the pore diameters and porous oxide layer thicknesses was investigated. The anodizing was carried out at 3.3 μms^{-1} scanning speed and six back and forth scanning times. The substrate temperature was controlled in the range of 10 ˚C to 60 ˚C. The temperature of the substrate during anodizing influences the diffusion of ions across the barrier oxide layer, and heat dissipation can occur at both interfaces. The surface SEM image of the porous AAO membrane formed with 0.3 M oxalic acid at various substrate temperatures and a constant applied voltage of 50 V in oxalic acid is shown in Fig. 2. The result shows that the consistency of the pores and morphology in the porous AAO membrane are significantly influenced by the substrate temperature. The pore regularity of the anodic alumina is improved by increasing the temperature of the substrate. The porous AAO membrane fabricated at 10 ˚C and 20 ˚C substrate temperatures shown in Fig. 2 (a) and (b) has a complete dis-order pore distribution. A small pore size and a slightly deformed porous AAO can be observed. The porous anodic oxide film grows slowly at these temperatures. The pore diameters and the neighboring pore distance are not uniform, and a significant variation in pore size is observed. This is because at a lower substrate temperature, the length of the pore is very

small due to the low dissolution rate of the barrier layer [25]. The rate of oxide formation at the metal/oxide interface and oxide layer dissolution at the electrolyte/oxide interface are increased with an increase in substrate temperature [26].

When the anodizing substrate temperature increased to 30 ˚C and 40 ˚C, the number of pores present significantly increased, and the pore became circular compared to the lowest substrate temperature, as shown in Fig. 2 (c) and (d), respectively. A porous oxide with uniform morphology is formed. The porous AAO membrane fabricated at 50 ˚C, shown in Fig. 2 (e), has a relatively well-ordered and uniform pore arrangement, while at 60 ˚C shown in Fig. 2 (f), a nearly perfect hexagonal pore arrangement with wide pores of the AAO membrane is observed. When the substrate temperature increased, the movement of electrolyte ions increased and the anodic oxide film on the Al was exposed to locally warm which enhanced the oxide dissolution to form regular pore structure. The order of the pores increases with an increase anodizing temperature because of heat dissipation, which is related to volume of expansion [27]. Many pore cells at higher substrate temperature are shown closed and connected to each other hexagonally in a regular configuration. The formation of uniform pore diameter and interpore distance to the neighboring pores and hexagonal pore arrangement are observed at higher substrate temperatures due to the high strengthening electric field across the barrier oxide layer at the pore base. The distance of the consecutive neighboring pores and their pore diameters show a consistent and uniformity under the analyzed area of the alumina line. The examined surface area shows that the pores have no defects. Further increased substrate temperature will enhance the dissolution rate of oxide layer, resulting in the collapse of the porous structure and the loss of its stability at the outer surface due to strong chemical dissolution [28].

The effect of substrate temperature on pore diameter, interpore distance, and porosity of porous AAO membranes is shown in Fig. 3. The average pore diameter and interpore distance were determined from SEM images for various anodizing substrate temperatures. The result shows that the temperature of the substrate significantly influences the pore diameter and slightly influences the interpore distance. The calculated porosity of the anodized area result shows the average porosity increases from 7% to 46% as the anodizing substrate temperature increases from 10 ˚C to 60 ˚C. The porosity reaches its highest value when the substrate is anodized at highest temperature due to an increase in pore diameter. It is reported that the temperature increased the rate of chemical dissolution of oxide layers during anodizing and resulted in widened pores on the surface of the oxide layer [29].

The current density temporal behavior as a function of substrate temperature anodizing in oxalic acid at a constant applied voltage is given in Fig. 4. The result shows that the current density increases as the substate temperature increase. The pore diameter slightly increases as the substrate temperature increase due to the field-assisted dissolution of the oxide layer initiated through higher current density at higher temperatures. The effect of anodized substrate temperature on the thickness of porous AAO membrane layer formed at 50 V in oxalic acid electrolyte is shown in Fig. 5. The result shows that at constant electrolyte temperature, the AAO membrane thickness initially increased and then decreased with increasing substrate temperature. The oxide film thickness increased as the anodizing temperature reached 30 ˚C. However, the film thickness decreased as the substrate temperature increased to 60 ˚C. The thicker oxide layer was formed at a substrate temperature of 30 ˚C. This can be explained by the fact that when the anodizing temperature increases, instantly the current density increases due to the declined of resistivity and resulting in a decrease in anodic porous layer growth. In addition, increasing substrate temperature

enhances the dissolution rate of the barrier-type oxide layer on the pore bottom side of substrates, causing a decline in the porous layer thickness. The porous AAO film thickness formed at 30 ˚C was considered the thickest oxide layer compared to other substrate temperatures. Further increased the substrate temperatures, resulting in a high degree of barrier oxide dissolution to form porous AAO. This results in a decrease in oxide layer thickness as the temperature of the substrate increases. During anodizing, the Al was remined in contact with the electrolyte droplet, and there was heat transfer from the substrate to the electrolyte droplet and vice versa. A thermal boundary layer was developed at the electrolyte/oxide interface under constant electrolyte temperature, resulting in a variation of the electrolyte droplet temperature from the surface oxide temperature, which was significantly different from the substrate-controlled temperature. In these ways, the level of oxide formation increased when the substrate temperature was higher than the electrolyte temperature. On the other hand, the opposite occurred when considering a low applied substrate temperature compared to the electrolyte temperature. When the anodizing was carried out in cooling environment with relatively low substrate temperatures of 10 ˚C and 20 ˚C, the growth rate of the local oxide layer was low as allied by the low current density. It is observed that at lower anodizing temperature, the rate of porous AAO film growth is due to the presence of a low and constant current density. However, as the temperature of the substrate was further increased to 30 ˚C, the level of oxide formation at the metal/oxide interface increased, and the thickness of the oxide layer increased. Further increasing the substrate temperature from 40 to 60 ˚C, the rate of chemical dissolution of the barrier oxide layer at the electrolyte/oxide interface was increased, which resulted in a decline in barrier oxide layer thickness, allowed for an increase in pore length. The thickness of the oxide barrier film considerably decreases and becomes thinner at the highest temperature due to the high level of chemical dissolution of the pore wall.

A similar result was reported by Theohari and Kontogeorgou [30] in their investigation of the anodizing of Al alloy AA5052 in sulfuric acid solution. The authors reported that increasing the anodization temperature up to 30 ˚C resulted in increase in porous film thickness. Reduction of thickness of barrier layer was resulted from the excessive dissolution of oxide into the electrolyte but further increased up to 40 ˚C showed a decline of anodic film thickness. The degree of barrier oxide film dissolution and formation increased with increasing local substrate temperatures. During anodizing process, the anodic current mainly encouraged the movement of Al ions from the metal surface [31]. The metal ions moved rapidly towards the metal/electrolyte interface to react with oxygen ions and form Al_2O_3. The dissolved ions mobility during oxidation of the Al surface decreased with increasing temperature. At higher anodizing temperatures, the oxidation level is high, which does not essentially increase the alumina film thickness but probably increases the chemical dissolution of the oxide layer in the electrolyte to form a porous alumina membrane [32]. The porous alumina layer formed at lower temperatures was thicker than that formed at higher temperatures due to the low level of chemical dissolution of the barrier oxide film at low temperature. While at higher temperature, the degree of oxide dissolution is faster to form a porous AAO membrane compared to the growth rate of the oxide layer, resulting in a decrease in film thickness. In general, a strong falling-off of the oxide layer thickness as a function of anodized temperature was observed at a constant electrolyte temperature. On the other hand, a thin anodic oxide thickness was noticed when the highest limiting thickness of the oxide layer was reached, which mainly appeared at the higher substrate temperature. It can be concluded that anodizing temperature played a major role in the fabrication of the desired porous alumina membrane film thickness for water purification applications.

Fig. 6 shows the cross-sectional images of the porous AAO membrane obtained through the one-step anodizing technique in oxalic acid at 50 V. The cross-sectional images of the oxide layer formed at a substrate temperature of 20 ˚C possessed a dense structure with small pore size and a slight oxide growth was developed, as shown in Fig. 6 (a). The pores are separated by thick pore walls and the layers are not well structured. By increasing the substrate temperature to 30 ˚C, the formation of a thick alumina membrane was increased. The pore structure became more open with increasing pore size. At this optimum anodized temperature, a normal Al_2O_3 layer with a compact microstructure was formed. A uniform and parallel with equal distance separated layered structures were fabricated, as shown in Fig. 6 (b). During the back-and-forth movement of the SF-MDC, several layered structures are formed with minor difference in film layered thickness as shown in Fig. 6 (c). The difference in layer thickness that occurred during the back-and-forth moving may be due to the narrow pore size formation and top surface dissolving. The anodized lines formed with SF-MDC exhibit a clearly visible and separated layered type of structure. The average layer thickness is about 3.1μm. Fig. 6 (e) and (f) show the fabricated oxide layered structure at anodizing temperatures of 50 ˚C and 60 ˚C, respectively. The anodized porous alumina layer contains a uniform and parallel cylindrical porous AAO membrane. The layered structure is clearly observed as the anodized temperature increased from 30 to 60 ˚C. However, at the lowest temperature, a layered structure is not clearly observed. The number of layers decreased as the substrate temperature increased. The number of cycles or repetitions conducted during anodization is equal to the number of layers formed. Each layer has a slight variation in film thickness due to the non-uniformity of droplets contact with substrate.

In this work, the influences of anodizing substrate temperature on the anodizing process for the formation of porous AAO membrane were deliberated through controlling and varying the

Al substrate temperature. The actual anodizing temperature is referenced as the temperature of the barrier layer of the porous AAO membrane. Both the electrolyte and substrate temperature affect the anodizing process. Direct measurement of the actual temperature at the barrier layer is not possible. Al has a high thermal conductivity property and there is a strong bond between the Al substrate and the barrier oxide layer. The electrolyte droplets are considered to have as smaller thermal conductivity, heat transfer inside the pore within the electrolyte mainly occurs through thermal conduction. Since the area of the pore is small, the electrolyte droplet diffusion in the pore is supposed to be stationary. Thus, the effect of electrolyte droplet temperature on the barrier oxide layer temperature is likely to be lower than that of the Al substrate temperature. These principles showed that anodizing substrate temperature has a higher significant influence on the rate of anodic oxide growth than the electrolyte temperature.

3.2. Fabrication of through-hole AAO membrane

The open-pore porous AAO membrane was fabricated by controlling the scanning speed and back-and forth movements of the substrate during anodizing. The top and bottom SEM images porous AAO membrane fabricated by anodizing Al in oxalic acid at 50 ˚C are shown in Fig. 7 (a) and (b). The pore diameters are uniform and consistent with each other. Similarly, the top and bottom SEM images of the porous AAO membrane fabricated at 60 ˚C is shown in Fig. 7 (c) and (d). The pore diameter of the anodic alumina membrane is slightly enlarged when the substrate temperature increases to 60 ˚C. A highly hexagonal ordered pore arrangement is confirmed to cover the entire anodized surface. Small pore diameters are observed on the back side of the SEM image, but the pore holes on the front side are larger in diameter. This implies that the pore size was not increased on the back side during through-hole formation, unlike in the chemical etching process. On the other hand, through-hole porous AAO membranes with smaller pore sizes can be obtained in the

present process compared to the conventional process because of the rapid through-hole without increasing the pore diameter with etching. The pore diameter and interpore distance are not significantly changed with the neighboring. The average pore size of the sample obtained at 50 ˚C and 60 ˚C anodized temperatures are 72.4 nm and 82.1 nm, respectively. The bottom view of the alumina film thickness shown in both samples were thin and transparent film with uniform porous structure. It is clearly seen that after the barrier oxide layer was completely removed, the through-hole porous anodic membrane was fabricated in both anodized temperatures. The average pore size for the bottom-through-hole alumina membrane at 50 ˚C and 60 ˚C is 33 nm and 38 nm, respectively. The through-hole alumina membrane with uniform morphology and small pore diameters can be fabricated at different anodizing substrate temperature without etching.

3.3. Effect of electrolyte composition on porous AAO membrane fabrication

Various electrolytes such as oxalic acid, phosphoric acid, and sulfuric acid were consequently conducted to investigate the pore structure of the anodized lines. The optical microscope images of the anodized lines with different electrolytes are shown in Fig. 8 (a). The anodized lines were conducted at room temperature and applied voltage of 50 V, 150 V and 25 V for $C_2H_2O_4$, H_3PO_4, and H_2SO_4, respectively. The results show that the anodized lines have equal length and width with different color appearances. The length of the anodized lines can be increased by controlling the movement of the XYZ moving stage, while the width of the anodized lines is directly related with the inlet and outlet flow rates of the electrolytes and the diameter of the inner capillary. The anodized areas in all electrolytes are clearly distinguishable from the Al substrate. The porous AAO line formed by each electrolyte has a different oxide color presence, such as light yellowish color (oxalic acid), a pale color (phosphoric acid) and a dark grayish color (sulfuric acid). The formation of colored oxide film during Al anodizing depends on the anodizing conditions and the

thickness of the anodic oxide layer. The surface SEM images of the anodized lines formed by different electrolytes are shown in Fig. 8 (b). The top surface images confirmed that the porous structure of anodized lines formed in various electrolyte solutions is different from each other. All anodized lines have a pore structure with differences in pore arrangement, pore size, and interpore distance. This is due to the presence of different electrolyte compositions and different supply current flows to the droplet of electrolyte contact with the substrate during anodizing.

The average pore diameter of the anodized lines formed at oxalic acid, phosphoric acid, and sulfuric acid at scanning of 3.3 μms^{-1} is 38.6 nm, 218 nm, and 19 nm, respectively. The results of average pore diameters obtained with SF-MDC are in good agreement with those obtained from previous studies [33]. The porosity of the anodized lines in different electrolyte solutions are calculated using Eq. (1). The corresponding average porosity of the anodized lines is 15.6 %, 48.8 %, and 10.6 % in oxalic acid, phosphoric acid, and sulfuric acid, respectively. Similarly, this result agrees with a previous study that reported the porosity of anodized lines prepared using SF-MDC at 0.3 M oxalic acid was estimated at 38 % [33]. The smallest pore diameter and interpore distance are recorded in sulfuric acid electrolyte while the largest pore size is obtained in phosphoric acid with the same electrolyte concentration. It should be noticed that the composition of the electrolyte significantly influences the pore diameter and interpore distance of the porous AAO membrane formed during the anodizing process. This variation in pore diameter is essential for the fabrication of membrane filters to separate solute molecules based on their molecular size.

The formation of pore structure during anodizing can be controlled and modified by controlling the anodizing parameters such as anodizing time, voltage, temperature, and electrolyte composition and concentration [34]. The cross-sectional SEM images of the anodized lines with different electrolytes are shown in Fig. 8 (c). All anodized lines have uniform cross-sectional,

layered structures. The thicknesses of the anodized lines are slightly different from each other, which is due to the use of different applied voltages. The AAO membranes comprise pores that are parallel, straight, and cover the whole membrane perpendicularly from the top side to the bottom surface. The barrier film thickness, pore size, and interpore distance formed under anodized phosphoric acid are larger than those of other electrolytes. The thickness of the anodized layer is related to the anodizing voltage. All anodized lines have a homogenous cross-sectional structure.

3.4. Fabrication of open-pore porous alumina at room temperature

The open-pore porous memebrnae can be fabricated by controlling the scanning speed to be 1.6 μms^{-1} and increasing the number of repetitions to eleven with various electrolytes at room temperature. Fig. 9 (a) shows the large-area SEM image of the top side of the through-hole porous AAO membrane formed by oxalic acid. The result shows that the porous membrane has a regular and hexagonal arrangement. The average pore size and interpore distance of the porous AAO membrane films are measured to be nearly 74 nm and 104 nm, respectively. The distance of the consecutive neighboring pores and their pore diameters show consistency and uniformity under the analyzed top area of the AAO line. The corresponding bottom SEM image of the anodized line with oxalic acid is shown in Fig. 9 (b). The through-holes are observed all over a broad area of the AAO layer, and such through-holes occur on the entire AAO membrane, including the top and bottom anodized lines. The pores consist of long and parallel cylindrical tubes of alumina layer with a uniform pore structure. Fig. 9 (d) and (e) show the top and bottom SEM views of the anodized porous AAO membrane formed in phosphoric acid, respectively. A uniform pore arrangement with a wide pore size is observed. The result shows that pore diameter and interpore distance are not varied mainly from one to the other. The average pore diameter and interpore distance of the porous AAO membrane are found to be approximately 218 nm and 297 nm,

respectively. The top surface image of the anodized lines in both electrolytes clearly shows a variation in pore diameter, suggesting a non-uniform supply of current to the droplet and nature of the electrolyte composition reactivity with the substrate. It is clearly shown that after the barrier oxide layer is dissolved and removed, the pores are completely opened at the bottom of the substrate. The result shows that the larger pore diameter was recorded during phosphoric acid anodizing. It can be clearly shown that the pore diameter of the top surface is slightly larger than that of the bottom-analyzed surface, indicating that the shape pore of the AAO membrane is likely a conical structure. The top surfaces of both AAO samples show honeycomb like structures with uniform pore diameters and consistent interpore distances. The pore diameter and interpore distance are not significantly different from the neighboring cells. The cross-sectional SEM images of the fabricated porous AAO membrane anodized in oxalic and phosphoric acid are shown in Fig. 9 (c) and (f), respectively. The result shows that uniform, straight, and parallel-order pore channels of AAO membranes were successfully fabricated on Al substrate at room temperature. The cross sections of anodized lines show uniform structural characteristics. The capability of SF-MDC to fabricate different pore sizes in various electrolytes creates an application in the field of membrane filter process. Thus, through-hole porous AAO membranes can be easily fabricated at room temperature without chemical etching or posttreatment using this technique in different electrolyte. Using the conventional anodizing method, it is not possible to fabricate an open-pore alumina membrane with a different porous structure. Over time, chemical etching could result in the collapse of nanotubes and reduce the alumina membrane thickness, resulting in low strength and durability. Hence, it is highly proposed for the fabrication of a higher pore arrangement of anodic alumina membrane using SF-MDC. Therefore, an effort is made to fabricate a through-hole porous

AAO membrane with different pore structures by varying the anodized temperature and electrolyte composition.

The mechanism of barrier oxide layer dissolution during through-hole pore AAO formation with SF-MDC is schematically shown in Fig. 10. At the initial stage of the anodizing process, the current line is distributed in the barrier oxide layer, as shown in Fig. 10 (a). The applied high voltage during anodizing is responsible for barrier oxide dissolution locally and enlargement of pores, as shown in Fig. 10 (c). At the middle stage of the anodizing process, the electrolyte remains in the pores during the scanning time and, the dissolution of barrier layer occurs. The oxide layer pore walls at the electrolyte/oxide interface dissolved locally due to chemical dissolution caused by increasing temperature [35]. After applying constant voltage, the barrier dissolution rate increased considerably, because of an increased electric field locally. Subsequently, an electrical breakdown of the crucial thinned oxide barrier film at the pore bottoms occurs, as shown in Fig. 10 (d). When the barrier oxide breakdown occurs, the electrolyte droplets penetrate the oxide/metal interface, as shown in Fig. 10 (e). The resistance of the barrier layer declined and dissolved at the given applied voltage and anodizing period. The oxide film does not grow on the metal surface because the dissolution rate of the barrier oxide is faster than its formation rate. Finally, a free standing through-hole porous AAO membrane with all pores open can be successfully fabricated from the Al surface.

The locally formed through-hole porous AAO layer was tested by putting Rhodamine B solution droplets on the anodized top side. The schematic representation of the top and bottom views of the anodized porous AAO membrane during Rhodamine B solution removal is shown in Fig. 11 (a). The results of the Rhodamine B diffusion towards porous AAO membrane on the anodized area at different time is exhibited. Fig. 11 (b) shows the initial contact time of 10 s of

Rhodamine B solution putting on top anodized alumina line. The result shows that the porous alumina is only present with a small dye solute component inside the pore of the membrane. After putting the solution on the alumina line and observed for 20 s, some pores are filled by the solute molecule, as shown in Fig. 11 (c). For long contact time of 60 s, all porous AAO membranes are occupied and filled by the dye molecule, as shown in Fig. 11 (d). A significant color change appeared when contact time was increased, indicated that the Rhodamine B dye solute molecules were spread into the anodized area to be retained in the porous wall structure. All pores then become occupied and filled by the solute molecule inside the membrane. The diameter of solute components that are larger than the pore membrane diameter will be retained through the pore of the membrane. The solution of the dye molecules is highly diffused to the pore of the bottom area and still needs extra pressure to flow out the solvent from the porous membrane. This result confirmed that the AAO membrane sample prepared in this study has through-hole porous AAO. Further use of pressure will enhance the separation of the solute components from the solution at the bottom of the anodized area. Hence, self-ordered through-hole porous AAO membrane is effectively fabricated at room temperature without chemical etching or post-treatment.

Based on the experimental results, it was confirmed that AAO membrane can be fabricated in a single step using the SF-MDC anodization technique. It is a simpler and more eco-friendly process for the fabrication of through-hole porous AAO membranes than other proposed conventional methods since oxide barrier films are easily removed without using chemical etching.

4. Conclusion

In this work, the effect of anodizing substrate temperature and composition of electrolytes on the formation of a through-hole porous AAO membrane at constant voltage with SF-MDC was studied. The anodizing substrate temperature greatly influenced the regularity of nanopore structure and

the degree of oxide film growth. Through-hole ordered porous AAO membrane was successfully fabricated at various substrate temperature and electrolyte composition without chemical etching using the SF-MDC technique. It was found that the pore size and order of the pore was significantly changed by increasing the anodizing substrate temperature. Uniform, straight, and parallel-order pore channels of AAO membranes were successfully fabricated on Al substrate at room temperature. The largest pore diameter and interpore distance were obtained in phosphoric whereas the smallest pore diameter and interpore distance were recorded in sulfuric acid electrolyte. The fabrication of a self-ordered controlled pore size through-hole membrane was successfully achieved with a single-step anodizing method for membrane filtration.

CRediT authorship contribution statement

Adane Adugna AYALEW: Conceptualization, Investigation, Writing-original draft.

Xiaole HAN: Visualization, Software, Writing-review & editing.

Masatoshi SAKAIRI: Conceptualization, Funding acquisition, Resources, Supervision, Writing-review & editing.

Acknowledgments

The authors would like to acknowledge funding from the Ministry of Education, Culture, Sports, Science, and Technology (MEXT), Japan. This work was also supported by JST SPRING, Grant Number JPMJSP2119.

References

[1] A. A. Ayalew, X. Han, K. Suzuki, S. Yoshida, and M. Sakairi, "Fabrication of Ni-microstructure through electrochemical deposition using 3D printed solution flow type microdroplet cell," *Mater Today Commun*, vol. 37, p. 107069, Dec. 2023, doi: 10.1016/j.mtcomm.2023.107069.

[2] V. Stasi *et al.*, "Aluminium pre-patterning for highly ordered nanoporous anodized alumina," *Photonics Nanostruct*, vol. 5, no. 2–3, pp. 136–139, Oct. 2007, doi: 10.1016/j.photonics.2007.07.009.

[3] K. Stokes, K. Clark, D. Odetade, M. Hardy, and P. Goldberg Oppenheimer, "Advances in lithographic techniques for precision nanostructure fabrication in biomedical applications," *Discover Nano*, vol. 18, no. 1, p. 153, Dec. 2023, doi: 10.1186/s11671-023-03938-x.

[4] X. Shi, W. Qing, T. Marhaba, and W. Zhang, "Atomic force microscopy - Scanning electrochemical microscopy (AFM-SECM) for nanoscale topographical and electrochemical characterization: Principles, applications and perspectives," *Electrochim Acta*, vol. 332, p. 135472, Feb. 2020, doi: 10.1016/j.electacta.2019.135472.

[5] C. Santana Santos, B. N. Jaato, I. Sanjuán, W. Schuhmann, and C. Andronescu, "Operando Scanning Electrochemical Probe Microscopy during Electrocatalysis," *Chem Rev*, vol. 123, no. 8, pp. 4972–5019, Apr. 2023, doi: 10.1021/acs.chemrev.2c00766.

[6] C. M. Siket, A. I. Mardare, M. Kaltenbrunner, S. Bauer, and A. W. Hassel, "Surface patterned dielectrics by direct writing of anodic oxides using scanning droplet cell microscopy," *Electrochim Acta*, vol. 113, pp. 755–761, Dec. 2013, doi: 10.1016/j.electacta.2013.07.114.

[7] L. Cicutto, J. Roche, and L. Arurault, “Local Anodizing of a Newly Prepared Aluminum Micrometric Disk,” *Nanomaterials*, vol. 12, no. 5, p. 845, Mar. 2022, doi: 10.3390/nano12050845.

[8] M. Sakairi, F. Nishino, and R. Itzinger, “Formation of layered structure porous-type anodic alumina films locally with a solution flow-type micro-droplet cell,” *Surface and Interface Analysis*, vol. 48, no. 8, pp. 921–925, Aug. 2016, doi: 10.1002/sia.5893.

[9] K. Sakata, M. Bilal, M. Sakairi, and T. Murata, “Local Electrochemical Measurements by 3D Printed Sf-MDC Equipped with Optical Microscope,” *J Electrochem Soc*, vol. 168, no. 6, p. 061505, Jun. 2021, doi: 10.1149/1945-7111/ac07c1.

[10] M. Bilal and M. Sakairi, “High throughput electrochemically driven metal microprinting with multicapillary droplet cell,” *Mater Today Commun*, vol. 26, p. 102053, Mar. 2021, doi: 10.1016/j.mtcomm.2021.102053.

[11] A. A. Ayalew, X. Han, and M. Sakairi, “A critical review of additive material manufacturing through electrochemical deposition techniques,” *Addit Manuf*, vol. 77, p. 103796, Sep. 2023, doi: 10.1016/j.addma.2023.103796.

[12] J. Kapusta-Kołodziej, A. Chudecka, and G. D. Sulka, “3D nanoporous titania formed by anodization as a promising photoelectrode material,” *Journal of Electroanalytical Chemistry*, vol. 823, pp. 221–233, Aug. 2018, doi: 10.1016/j.jelechem.2018.06.014.

[13] H. Singh, P. Saxena, and Y. M. Puri, “The manufacturing and applications of the porous metal membranes: A critical review,” *CIRP J Manuf Sci Technol*, vol. 33, pp. 339–368, May 2021, doi: 10.1016/j.cirpj.2021.03.014.

[14] L. Zaraska, W. J. Stępniowski, E. Ciepiela, and G. D. Sulka, “The effect of anodizing temperature on structural features and hexagonal arrangement of nanopores in alumina

synthesized by two-step anodizing in oxalic acid," *Thin Solid Films*, vol. 534, pp. 155–161, May 2013, doi: 10.1016/j.tsf.2013.02.056.

[15] A. P. Leontiev, I. V. Roslyakov, and K. S. Napolskii, "Complex influence of temperature on oxalic acid anodizing of aluminium," *Electrochim Acta*, vol. 319, pp. 88–94, Oct. 2019, doi: 10.1016/j.electacta.2019.06.111.

[16] M. Schneider, C. Lämmel, C. Heubner, and A. Michaelis, "In situ temperature measurement on the metal/oxide/electrolyte interface during the anodizing of aluminum," *Materials and Corrosion*, vol. 64, no. 1, pp. 60–68, Jan. 2013, doi: 10.1002/maco.201106129.

[17] K. Chernyakova, B. Tzaneva, I. Vrublevsky, and V. Videkov, "Effect of Aluminum Anode Temperature on Growth Rate and Structure of Nanoporous Anodic Alumina," *J Electrochem Soc*, vol. 167, no. 10, p. 103506, Jan. 2020, doi: 10.1149/1945-7111/ab9d65.

[18] T. Aerts, I. De Graeve, and H. Terryn, "Control of the electrode temperature for electrochemical studies: A new approach illustrated on porous anodizing of aluminium," *Electrochem commun*, vol. 11, no. 12, pp. 2292–2295, Dec. 2009, doi: 10.1016/j.elecom.2009.10.013.

[19] Y.-C. Chien and H. C. Weng, "Cost-effective technique to fabricate a tubular through-hole anodic aluminum oxide membrane using one-step anodization," *Microelectron Eng*, vol. 247, p. 111589, Jul. 2021, doi: 10.1016/j.mee.2021.111589.

[20] J. Cui, Y. Wu, Y. Wang, H. Zheng, G. Xu, and X. Zhang, "A facile and efficient approach for pore-opening detection of anodic aluminum oxide membranes," *Appl Surf Sci*, vol. 258, no. 14, pp. 5305–5311, May 2012, doi: 10.1016/j.apsusc.2012.01.099.

[21] M. Sakairi, F. Sato, Y. Gotou, K. Fushimi, T. Kikuchi, and H. Takahashi, "Development of a novel microstructure fabrication method with co-axial dual capillary solution flow type

droplet cells and electrochemical deposition," *Electrochim Acta*, vol. 54, no. 2, pp. 616–622, Dec. 2008, doi: 10.1016/j.electacta.2008.07.017.

[22] M. Bilal and M. Sakairi, "3D printed solution flow type microdroplet cell for simultaneous area selective anodizing," *J Adv Res*, vol. 26, pp. 43–51, Nov. 2020, doi: 10.1016/j.jare.2020.06.019.

[23] C. A. Schneider, W. S. Rasband, and K. W. Eliceiri, "NIH Image to ImageJ: 25 years of image analysis," *Nat Methods*, vol. 9, no. 7, pp. 671–675, Jul. 2012, doi: 10.1038/nmeth.2089.

[24] A. Eftekhari, Ed., *Nanostructured Materials in Electrochemistry*. Wiley, 2008. doi: 10.1002/9783527621507.

[25] A. Ruiz-Clavijo, O. Caballero-Calero, and M. Martín-González, "Revisiting anodic alumina templates: from fabrication to applications," *Nanoscale*, vol. 13, no. 4, pp. 2227–2265, 2021, doi: 10.1039/D0NR07582E.

[26] B. Sellarajan, M. Sharma, S. K. Ghosh, H. S. Nagaraja, H. C. Barshilia, and P. Chowdhury, "Effect of electrolyte temperature on the formation of highly ordered nanoporous alumina template," *Microporous and Mesoporous Materials*, vol. 224, pp. 262–270, Apr. 2016, doi: 10.1016/j.micromeso.2015.12.045.

[27] R. A. Mirzoev, A. D. Davydov, S. I. Vystupov, and T. B. Kabanova, "Conditions for self-ordering of porous structure of anodic aluminum oxide in weak and strong acids," *Electrochim Acta*, vol. 294, pp. 276–285, Jan. 2019, doi: 10.1016/j.electacta.2018.10.041.

[28] T. Aerts, J.-B. Jorcin, I. De Graeve, and H. Terryn, "Comparison between the influence of applied electrode and electrolyte temperatures on porous anodizing of aluminium,"

Electrochim Acta, vol. 55, no. 12, pp. 3957–3965, Apr. 2010, doi: 10.1016/j.electacta.2010.02.044.

[29] G. D. Sulka and K. G. Parkoła, "Temperature influence on well-ordered nanopore structures grown by anodization of aluminium in sulphuric acid," *Electrochim Acta*, vol. 52, no. 5, pp. 1880–1888, Jan. 2007, doi: 10.1016/j.electacta.2006.07.053.

[30] S. Theohari and Ch. Kontogeorgou, "Effect of temperature on the anodizing process of aluminum alloy AA 5052," *Appl Surf Sci*, vol. 284, pp. 611–618, Nov. 2013, doi: 10.1016/j.apsusc.2013.07.141.

[31] L. Sacco, I. Florea, and C.-S. Cojocaru, "Fabrication of porous anodic alumina (PAA) templates with straight pores and with hierarchical structures through exponential voltage decrease technique," *Surf Coat Technol*, vol. 364, pp. 248–255, Apr. 2019, doi: 10.1016/j.surfcoat.2019.02.086.

[32] T. Kikuchi, M. Yamashita, M. Iwai, and R. O. Suzuki, "Self-Ordering of Porous Anodic Alumina Fabricated by Anodizing in Chromic Acid at High Temperature," *J Electrochem Soc*, vol. 168, no. 9, p. 093501, Sep. 2021, doi: 10.1149/1945-7111/ac2101.

[33] M. Bilal and M. Sakairi, "Fast Fabrication of Localized Porous Alumina Patterns with 3D Printed Microdroplet Cell," *J Electrochem Soc*, vol. 167, no. 8, p. 081501, Apr. 2020, doi: 10.1149/1945-7111/ab8877.

[34] W. Lee and S.-J. Park, "Porous Anodic Aluminum Oxide: Anodization and Templated Synthesis of Functional Nanostructures," *Chem Rev*, vol. 114, no. 15, pp. 7487–7556, Aug. 2014, doi: 10.1021/cr500002z.

[35] J. Oh and C. V. Thompson, “The role of electric field in pore formation during aluminum anodization,” *Electrochim Acta*, vol. 56, no. 11, pp. 4044–4051, Apr. 2011, doi: 10.1016/j.electacta.2011.02.002.

Figure Captions

Fig. 1. Schematic representations of an experimental setup for SF-MDC anodizing with aluminum substrate temperature control device.

Fig. 2. SEM images of the surface of porous AAO films fabricated with 0.3 M oxalic acid at aluminum substrate temperature of (a) 10 ˚C, (b) 20 ˚C, (c) 30 ˚C, (d) 40 ˚C, (e) 50 ˚C, and (f) 60 ˚C.

Fig. 3. Effect of aluminum substrate temperature on pore diameter (Dp), interpore distance (Din), and porosity (P) of AAO membrane.

Fig. 4. Current density as function of aluminum substrate temperature.

Fig. 5. Effect of aluminum substrate temperature on the thickness of the porous AAO membrane film formed with 0.3 M oxalic acid at 50 V and 3.3 μms^{-1} scanning speed.

Fig. 6. SEM images of a cross section of a porous AAO film formed with 0.3 M oxalic acid at aluminum substrate temperatures of (a) 20 ˚C, (b) 30 ˚C, (c, d) 40 ˚C, (e) 50 ˚C, and (f) 60 ˚C.

Fig. 7. SEM images of the anodized porous AAO film formed with 0.3 M oxalic acid at aluminum substrate temperature of 50 ˚C (a) top view, (b) bottom view, and 60 ˚C (c) top view and (d) bottom view.

Fig. 8. Fabrication of porous AAO films with 0.3 M oxalic acid, phosphoric acid and sulfuric acid electrolytes and applied voltage of 50 V, 150 V and 25 V, respectively shows (a) optical microscope images of anodized lines, (b) top-surface SEM images, and (c) cross-section images of anodized lines.

Fig. 9. SEM images of through-hole porous AAO membrane fabricated at room temperature with oxalic acid (a) top view, (b) bottom view, and (c) cross-section, and with phosphoric acid (d) top view, (e) bottom view, and (f) cross-section view.

Fig. 10. Mechanism of barrier layer dissolution during through-hole porous AAO film fabrication (a-e).

Fig. 11. Schematic represntaion of (a) top and back view of porous AAO membrane during Rhodamine B dye removal, and digital image of porous AAO back side view during Rhodamine B solution removal after contact time of (b) 10 s, (c) 20 s, and (d) 60 s.

Figures

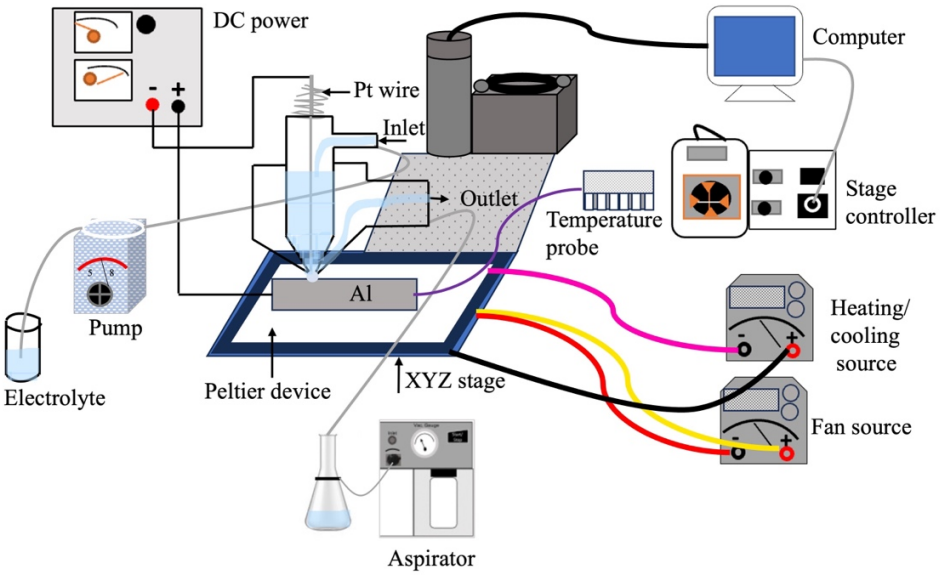

Fig. 1. Schematic representations of an experimental setup for SF-MDC anodizing with aluminum substrate temperature control device.

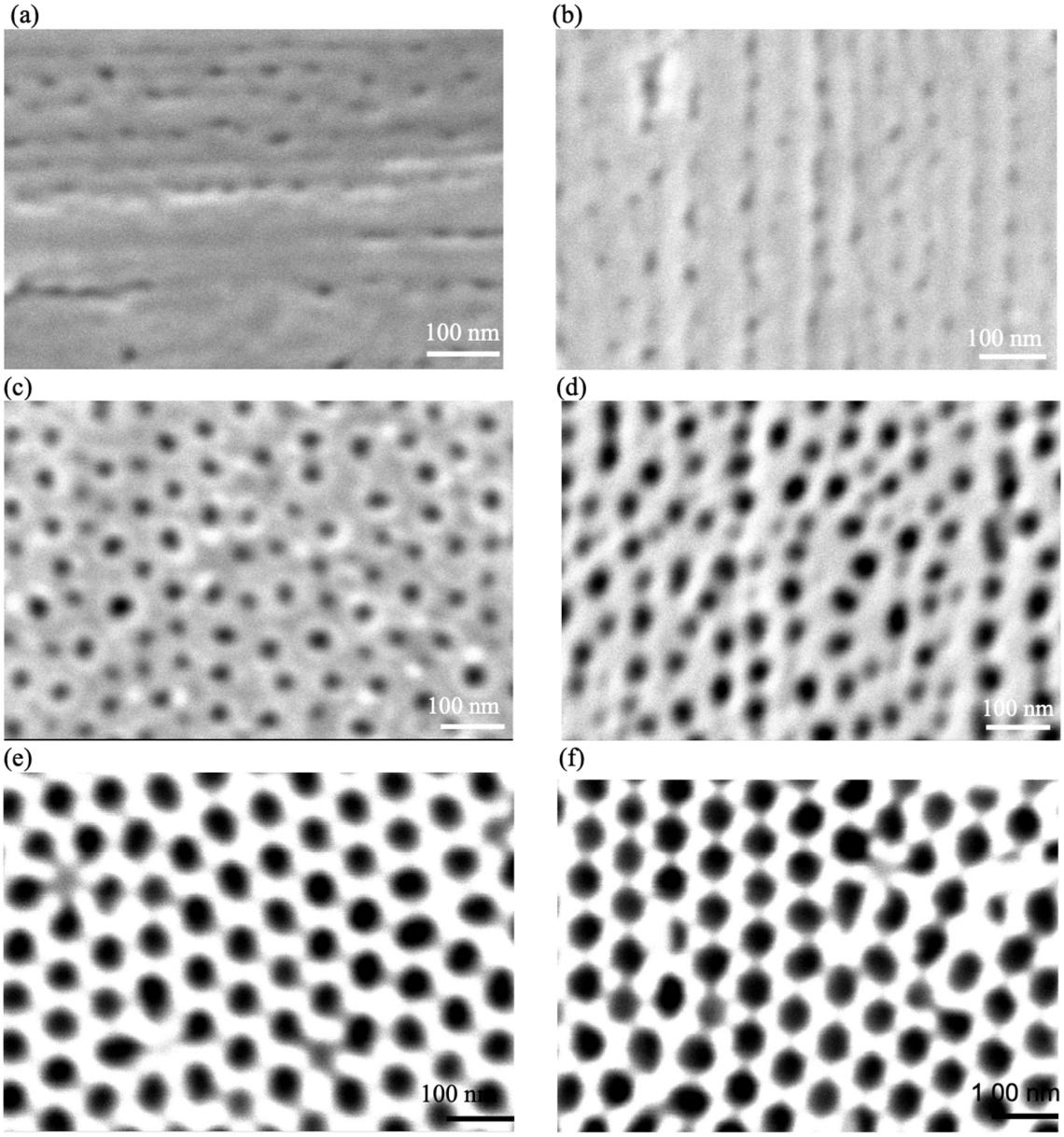

Fig. 2. SEM images of the surface of porous AAO films fabricated with 0.3 M oxalic acid at aluminum substrate temperature of (a) 10 ˚C, (b) 20 ˚C, (c) 30 ˚C, (d) 40 ˚C, (e) 50 ˚C, and (f) 60 ˚C.

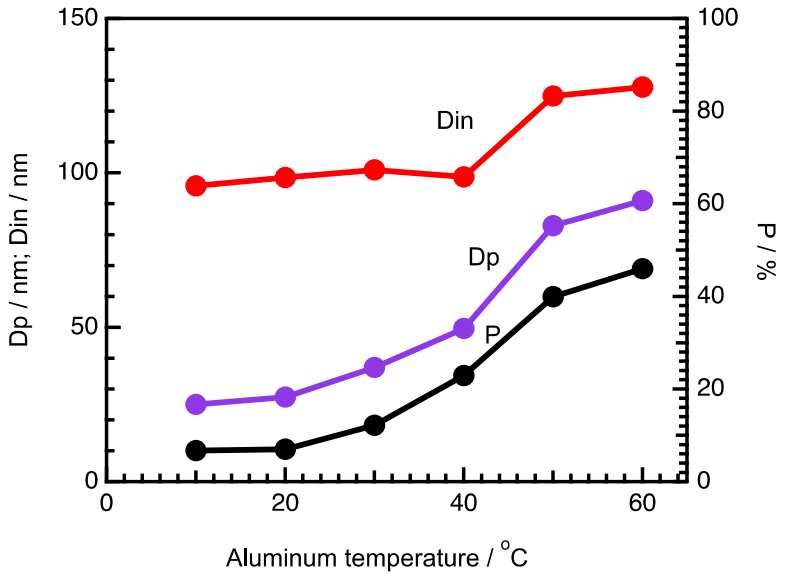

Fig. 3. Effect of aluminum substrate temperature on pore diameter (Dp), interpore distance (Din), and porosity (P) of AAO membrane.

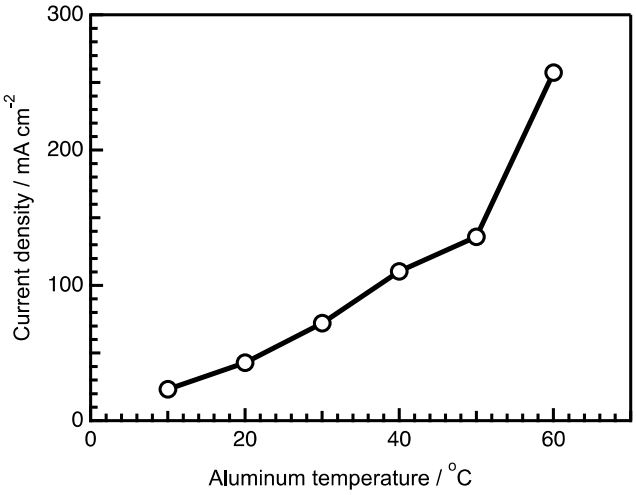

Fig. 4. Current density as function of aluminum substrate temperature.

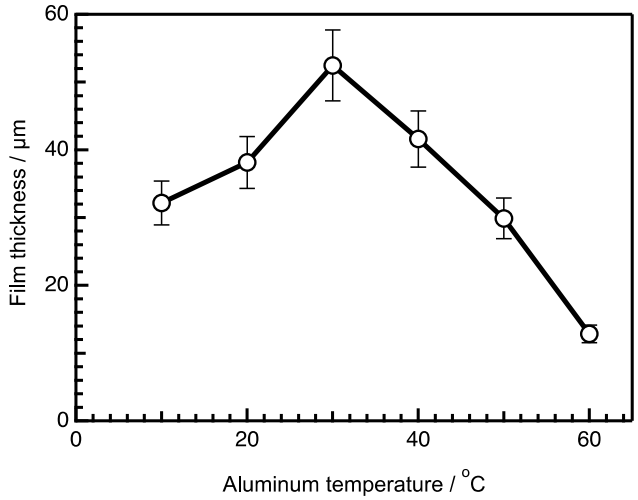

Fig. 5. Effect of aluminum substrate temperature on the thickness of the porous AAO membrane film formed with 0.3 M oxalic acid at 50 V and 3.3 μms^{-1} scanning speed.

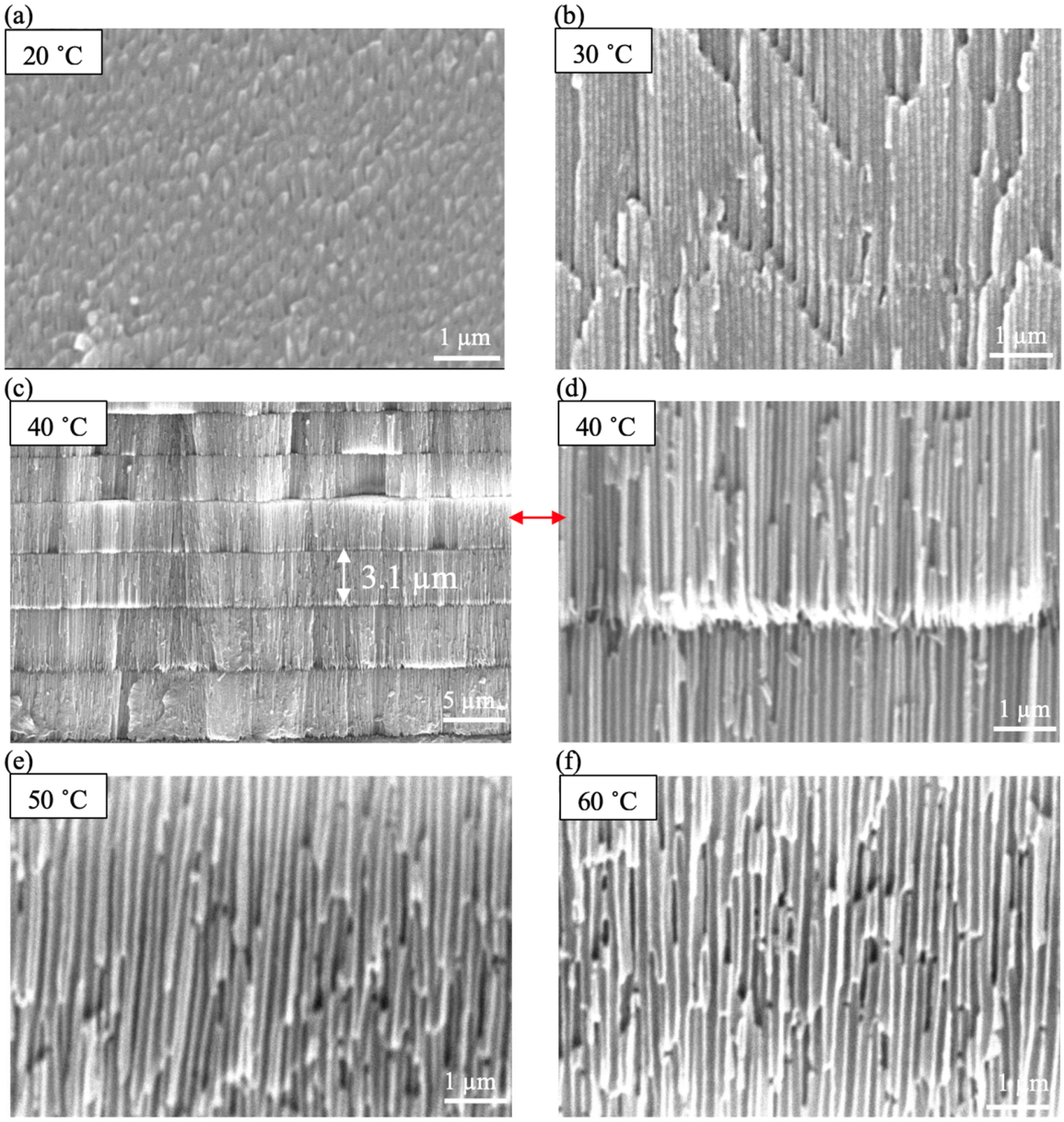

Fig. 6. SEM images of a cross section of a porous AAO film formed with 0.3 M oxalic acid at aluminum substrate temperatures of (a) 20 ˚C, (b) 30 ˚C, (c, d) 40 ˚C, (e) 50 ˚C, and (f) 60 ˚C.

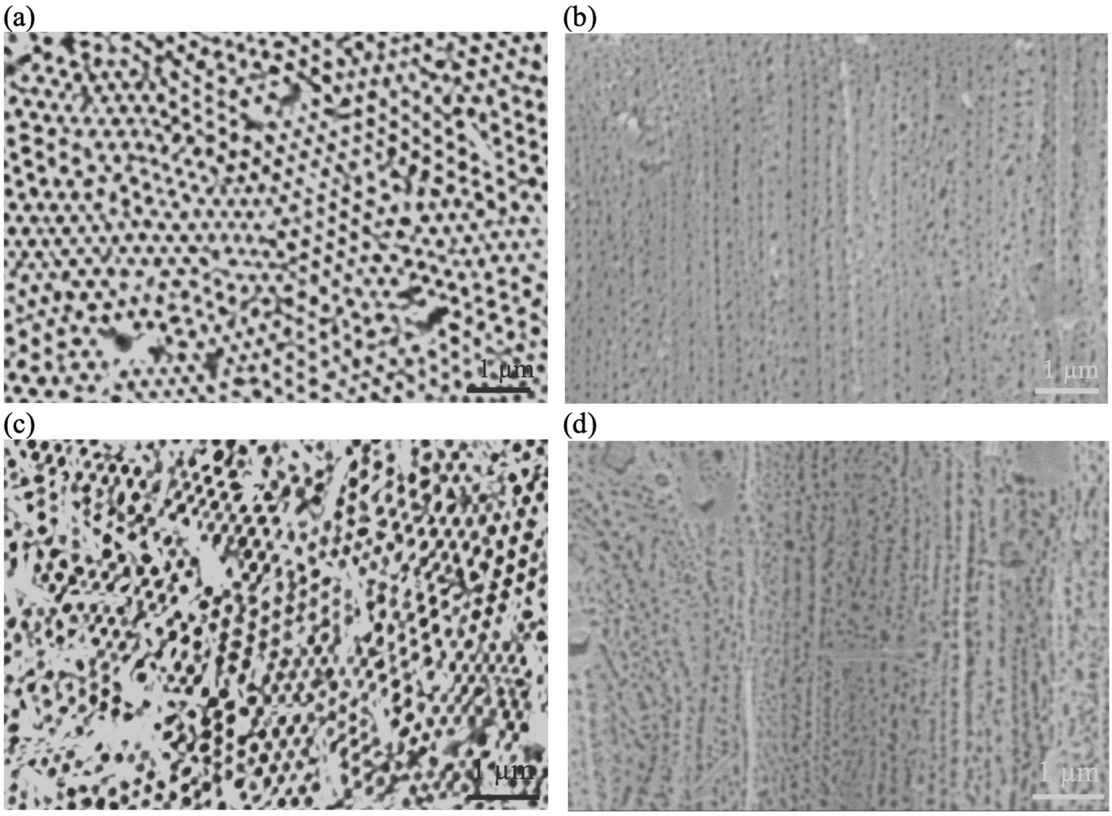

Fig. 7. SEM images of the anodized porous AAO film formed with 0.3 M oxalic acid at aluminum substrate temperature of 50 ˚C (a) top view, (b) bottom view, and 60 ˚C (c) top view and (d) bottom view.

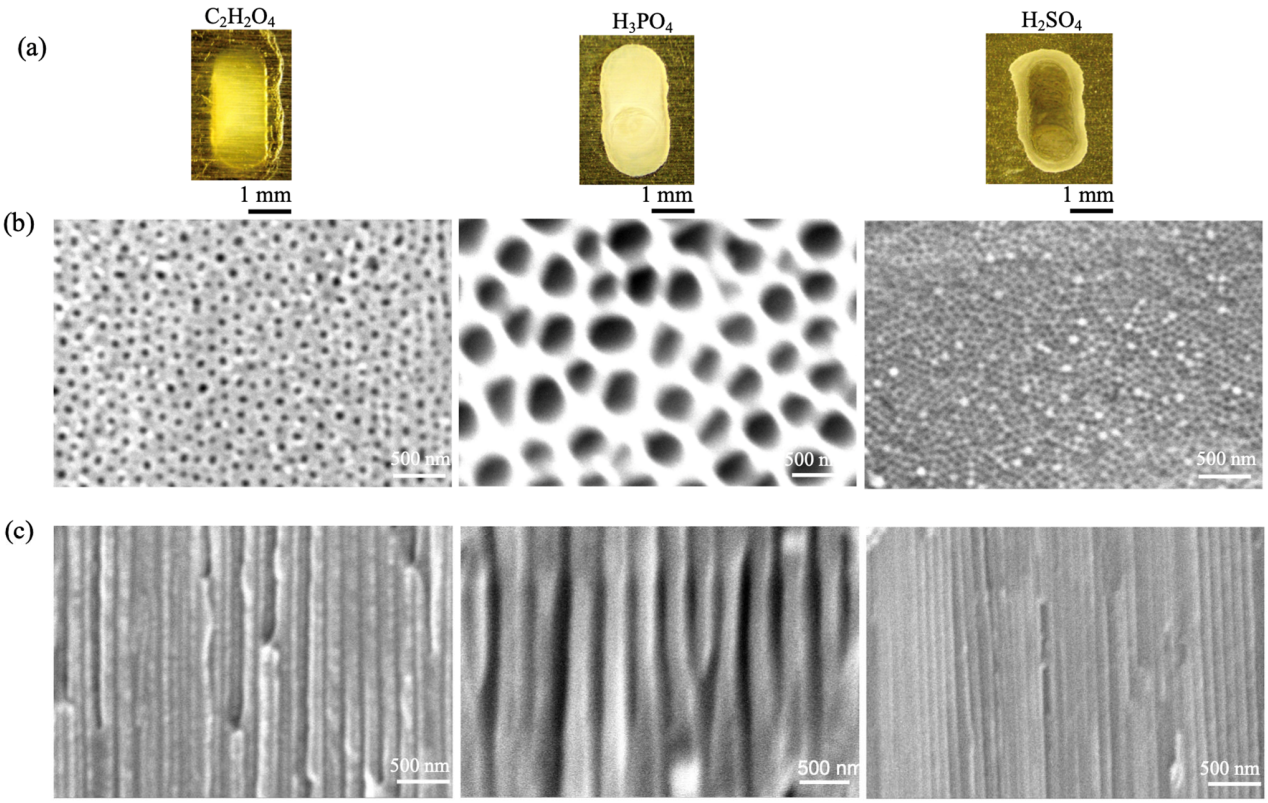

Fig. 8. Fabrication of porous AAO films with 0.3 M oxalic acid, phosphoric acid and sulfuric acid electrolytes and applied voltage of 50 V, 150 V and 25 V, respectively shows (a) optical microscope images of anodized lines, (b) top-surface SEM images, and (c) cross-section images of anodized lines.

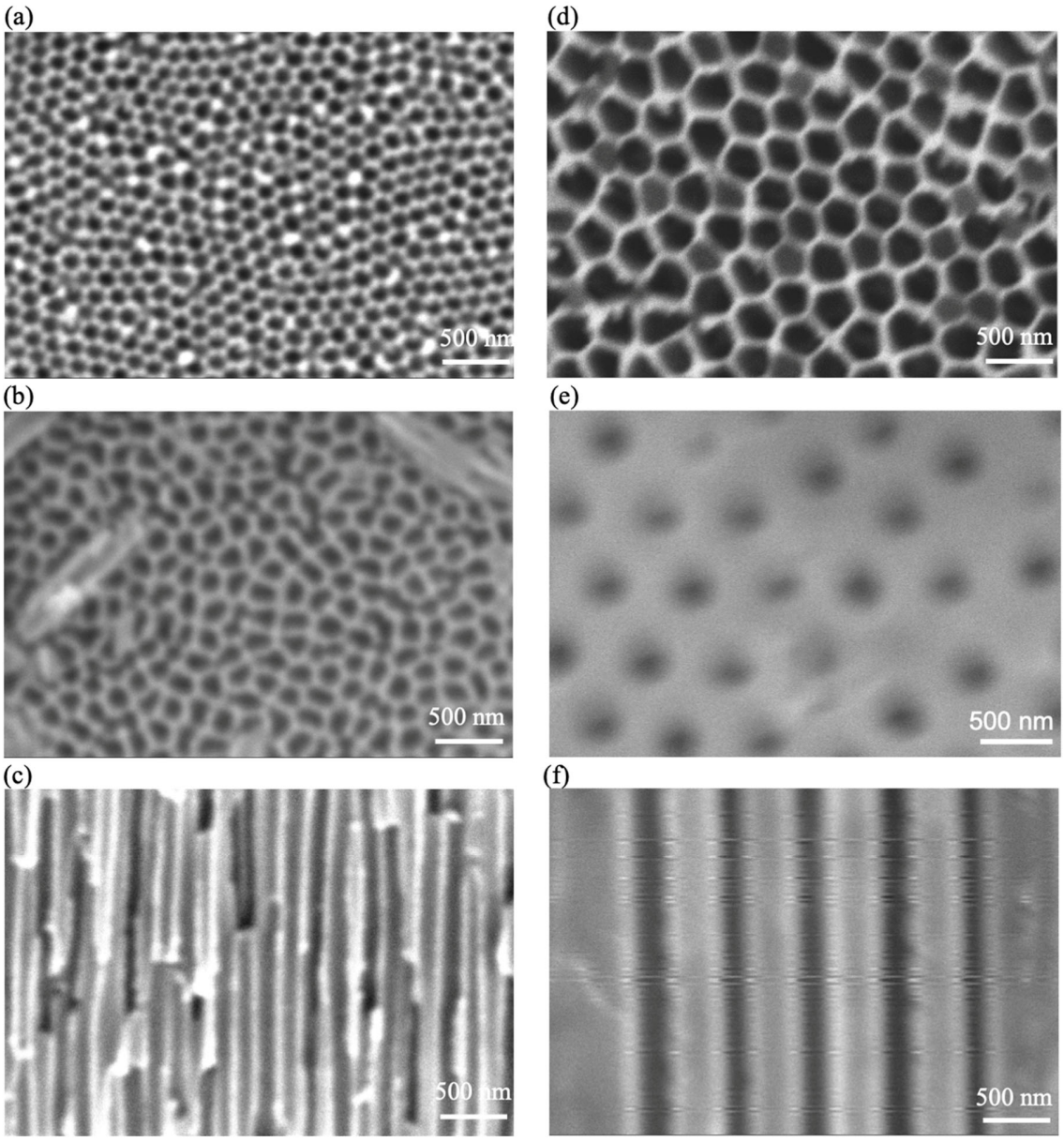

Fig. 9. SEM images of through-hole porous AAO membrane fabricated at room temperature with oxalic acid (a) top view, (b) bottom view, and (c) cross-section, and with phosphoric acid (d) top view, (e) bottom view, and (f) cross-section view.

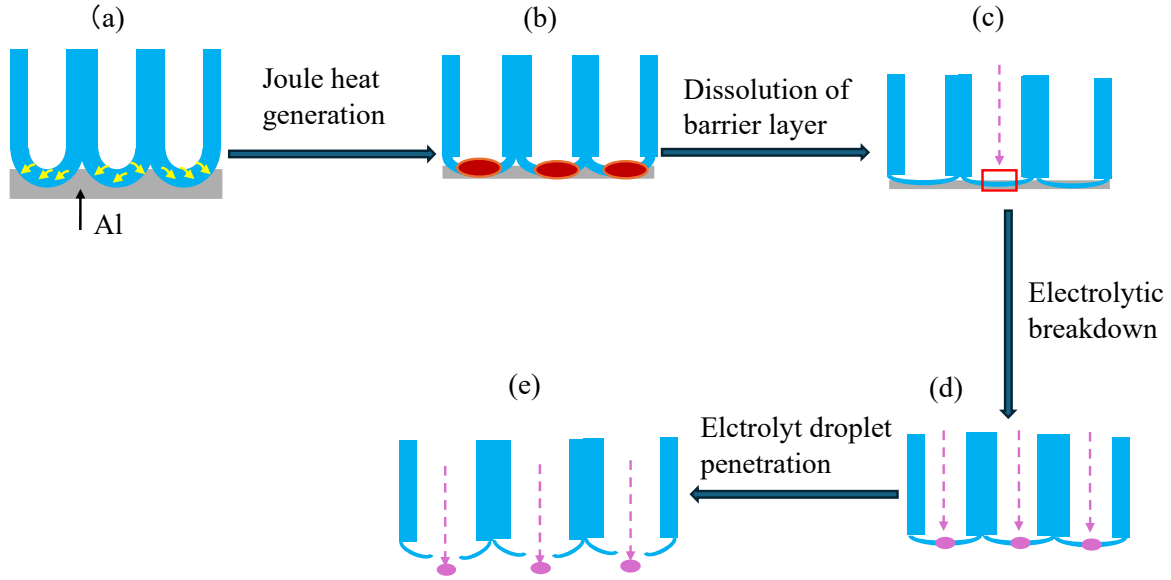

Fig. 10. Mechanism of barrier layer dissolution during through-hole porous AAO film fabrication (a-e).

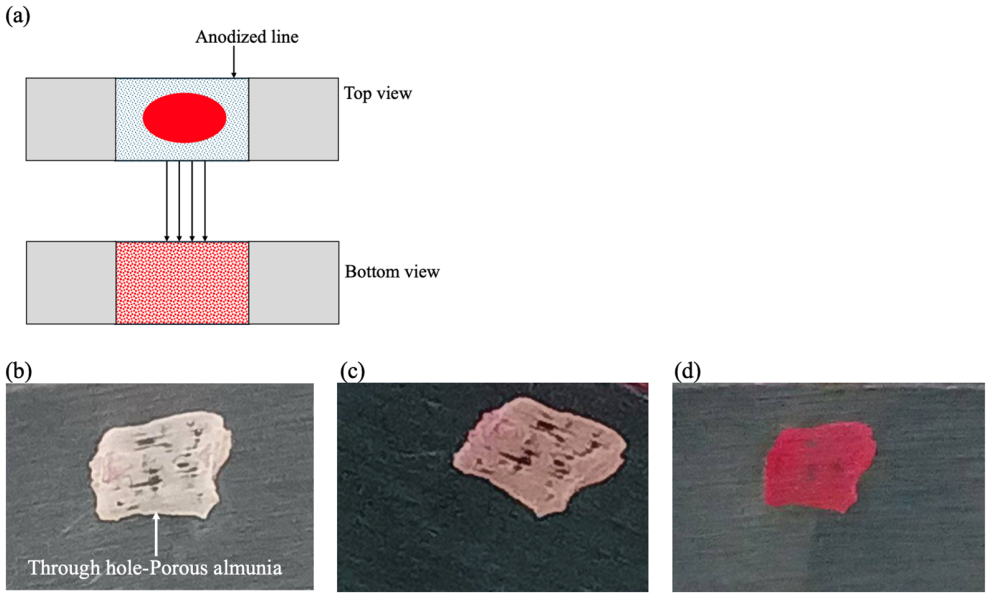

Fig. 11. Schematic represntaion of (a) top and back view of porous AAO membrane during Rhodamine B dye removal, and digital image of porous AAO back side view during Rhodamine B solution removal after contact time of (b) 10 s, (c) 20 s, and (d) 60 s.